DOI: 10.1002/ejic.200900587

A New Organic-Inorganic Hybrid Supermicroporous Material Having Luminescence and Ion-Exchange Property

Debraj Chandra,[a] Arghya Dutta,[a] and Asim Bhaumik*[a]

Keywords: Sensors / Fluorophore / Fluorescence / Ion exchange / Microporous materials / Organic-inorganic hybrid composites

A new crystalline microporous organic-inorganic hybrid material containing a diimine fluorophore inside the framework has been synthesized solvothermally without using any template or structure-directing agent (SDA). Powder XRD and N_2 sorption analyses suggested the formation of a new triclinic phase and supermicropores of dimension 1.39–1.53 nm in this material. ^{13}C CP MAS, ^{29}Si MAS NMR, UV/Vis absorption and PL spectroscopic results suggested the presence of bridging organic diimine fluorophore in this new porous framework. Due to the use of sole fluorophore organosilane moiety in this organic-inorganic hybrid framework, this material shows very large affinity toward metal cations like Fe^{3+}, Zn^{2+}, Cd^{2+} and Hg^{2+}, and thus can be efficiently utilized as metal ion chemosensor and exchanger. All the metal ion-exchanged samples show very strong photoluminescence at room temperature and strong dependence of emission colors when exchanged with a particular metal cation.

Introduction

Periodic mesoporous organosilicas (PMOs) and related organic-inorganic hybrid materials[1–3] have gained considerable interest over the years due to their exceptionally high surface area and possibility to incorporate a variety of organic functional groups in the pore walls, which could lead to many novel applications. Unique structural features of the functionalized mesoporous materials make them potentially useful in a wide range of advanced applications, e.g. chiral recognition,[4] sensing,[5] catalysis,[6] etc. Interestingly, for the syntheses of the microporous and mesoporous materials single molecule template[7] or supramolecular assemblies of the surfactant molecules,[8,9] which can act as the structure-directing agent (SDA) through electrostatic or H-bonding interactions with the frameworks is essential. Templating pathways for supramolecular assembly of surfactants in the synthesis of novel mesoporous materials have made a significant contribution in designing a large variety of mesoporous materials. Interestingly, the pore size of these materials is much larger than those attainable in zeolites[7] and this could be tuned on the nanometer scale by proper choice of the surfactant templating system, sometimes in association with a co-solvent or swelling agent during the synthesis.

Initial interest in this area of research is mainly focused to their potential use as adsorbent agents and catalysts because of the wide range of available pore sizes, high surface area and thermal stability. However, the high surface area of these materials allows high doping concentrations of the framework species and the tunable size range allows access to a variety of quantum-confined structures, which could have wide applications in sensing[5] and optoelectronics.[10] Thus a considerable research has been carried out in this context to develop nanoporous materials for optical sensors and related optoelectronic applications. A unique approach to sense the emission color from the solid materials is to graft a fluorophore[11] into an organic-inorganic hybrid PMOs.[12,13] PMOs and related silica-based hybrid materials have been synthesized from a wide range of bridging organosilane precursors (Figure 1), where two trialkoxysilyl groups are connected by an organic bridge. For this purpose, a variety of bulky organic functional molecules such as ethane, benzene, isocyanurate, phenolic imine, etc. are grafted or incorporated inside the channel of mesoporous materials. The design and synthesis of these innovative hybrid materials are of considerable interest and opens up a new and promising field of investigation for sensing and exchange of metal cations from solution.

Since the removal of these SDAs from these as-prepared porous materials to generate porosity is not very straightforward and so often removal of the template causes collapse of the pore apertures and channels, synthesis of novel porous materials without the aid of any SDA is highly desirable. However, there are only few reports on the synthesis of extra large pore or supermicroporous (having pore di-

[a] Department of Materials Science, Indian Association for the Cultivation of Science,
Jadavpur, Kolkata 700032, India
E-mail: msab@iacs.res.in

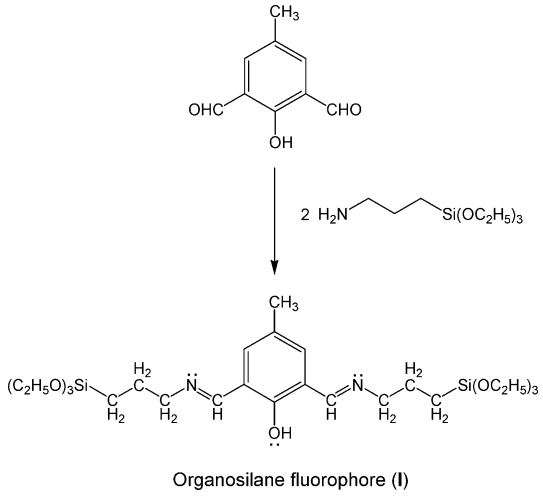

Figure 1. Synthesis of organosilane precursor (**I**) through Schiff base condensation between DFP and APTES.

mensionin the range of 1.0–2.0 nm) material[14] without using any SDA. Herein, we first report the sensing and ion-exchange properties of a luminescent organic-inorganic hybrid supermicroporous material LHMM-1, containing a fluorophore diimine moiety covalently grafted inside the framework without using any SDA solvothermally under strongly acidic pH condition. The emission wavelength of this material can be tuned in the presence of various biologically and environmentally demanding metal cations. The tuning ability of the PL band in the presence of different counter cations and high ion-exchange efficiency due to the presence of the chelating donor sites of the bridging diimine unit in the framework of a high surface area material are most remarkable features of this work. We believe that our synthetic strategy for hybrid frameworks through non-templating pathway would be widely applicable for the synthesis of a large variety of related porous materials, which could have many other potential applications.

Results and Discussion

Characterizations of LHMM-1

In Figure 2 we have shown the scanning electron microscopic images of LHMM-1 sample at different magnifications. Clear rectangular particle edges are seen for these samples. Particle sizes vary from 20–100 nm. In some places of the specimens it is further revealed that few tiny particles of ca. 10 nm sizes are agglomerated to form larger particles. The powder X-ray diffraction patterns for LHMM-1 samples (as-synthesized and NH_3 treated) are shown in Figure 3. Both samples show multiple diffractions corresponding to that shown by the crystalline microporous materials.[15] This powder diffraction peaks can be assigned very well with a new triclinic phase having the following unit cell parameters: a = 14.455 Å; b = 13.892 Å; c = 12.99 Å; α = 87.95°, β = 90.38° and γ = 91.36°. The unit cell volume for this triclinic hybrid material is quite large: V = 2603.73 Å^3; *hkl* for different planes and the respective d spacings are given in Table 1. It is interesting to note that this diffraction pattern does not match with any crystalline phase reported in the JCPDS files. PXRD pattern of the sample has been evaluated with the PXRD pattern calculated by using Reflex, a software package for crystal determination. The CELSIZ program was used to obtain the lattice parameters along with estimated standard deviations (esd, see Table 1). Very small deviations are in accord with a good fit of the calculated values with the experimental data. Thus, this powder XRD result suggests that LHMM-1 has a new organosilica framework structure.

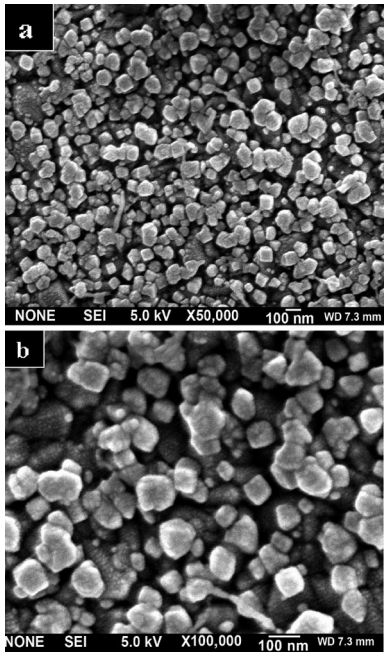

Figure 2. Scanning electron micrographs of LHMM-1 sample 2 (a and b) at different magnifications.

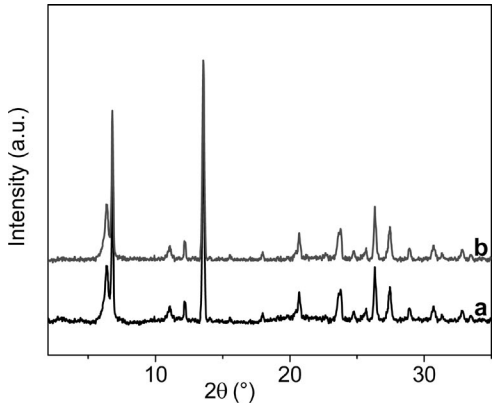

Figure 3. Wide angle powder XRD patterns of LHMM-1 samples 1 (a) and 2 (b).

To illustrate the thermal stability of LHMM-1 material, TG-DTA analysis of the sample 2 has been carried out under N_2 flow. TG and DTA plots for this material are shown in Figure 4. As seen from this Figure that LHMM-1 is stable upto ca. 403 K. Above this temperature organic frag-

Table 1. Unit cell parameters of LHMM-1.

Phase: triclinic Parameters			Deviations	
a = 14.455 Å			0.027	
b = 13.892 Å			0.013	
c = 12.990 Å			0.018	
α = 87.95°			0.11	
β = 90.38°			0.14	
γ = 91.36°			0.11	
V = 2603.73 Å^3			esd 5.0720	
h	k	l	2 theta [°]	d
0	1	0	6.362	13.880
0	0	1	6.803	12.982
1	–1	1	11.091	7.971
2	0	0	12.239	7.225
0	0	2	13.631	6.491
1	–2	1	15.608	5.673
2	2	0	17.915	4.947
2	2	–1	19.157	4.629
1	2	–2	19.762	4.489
3	–1	1	20.565	4.315
3	–1	2	23.805	3.735
2	–1	–3	24.667	3.606
0	4	0	25.651	3.470
1	–4	0	26.248	3.392
1	4	1	27.436	3.248
1	–3	3	28.822	3.095
2	–3	3	30.718	2.908
3	–4	0	31.387	2.848
2	–2	4	32.809	2.727
1	–4	–3	33.516	2.672

ment comes out with multiple exothermic peaks in the temperature range 423–953 K. This result has prompted us to carry out the degassing of these samples at 393 K in the N_2 sorption experiments.

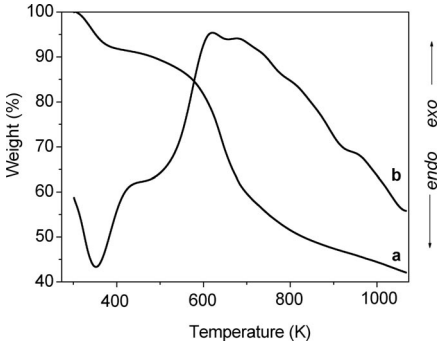

Figure 4. TG (a) and DTA (b) plots for LHMM-1 acid-treated sample 2.

BET surface areas, average pore diameters and micropore volumes for LHMM-1 samples estimated from their respective adsorption isotherms are given in Table 2. The N_2 adsorption/desorption isotherms of as-synthesized and ammonia-treated samples are shown in Figure 5 (A). These isotherms can be classified as type I characteristic of the microporous materials.[7] The sharp increase in N_2 uptake for very low P/P_0 is suggesting the presence of large micropores in these samples. Pore size distribution of these samples estimated by employing the NLDFT method is shown in Figure 5 (B). The BET surface area of ammonia-treated hybrid sample increased from 92 to 459 $m^2 g^{-1}$. Enhanced surface area for sample 2 vis-à-vis sample 1 suggested that the deprotonation via NH_3 treatment helps to remove the counter anions from the protonated imine species present in the framework. Pore volume also enhanced during ammonia-treatment from 0.09 ccg^{-1} to 0.29 ccg^{-1} (Table 2). However, average pore width has been decreased from about 1.53 to ca. 1.39 nm.

Table 2. Physico-chemical properties of LHMM-1 materials.

Sample number	BET surface area [$m^2 g^{-1}$]	Pore diameter[a] [nm]	Pore volume [ccg^{-1}]
1 (as-synthesized)	92	1.53	0.09
2 (NH_3-treated)	459	1.39	0.29

[a] Estimated by the NLDFT method (Figure 5, B).

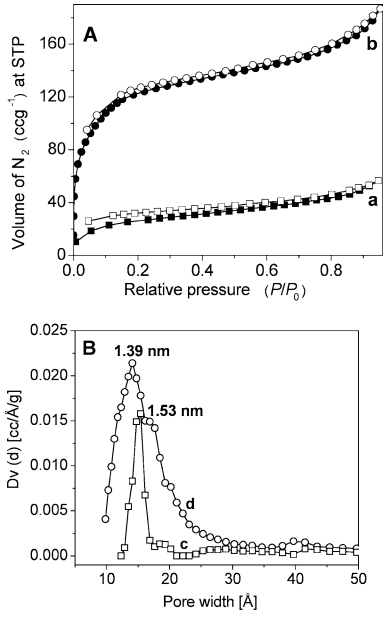

Figure 5. A: N_2 adsorption/desorption isotherms of LHMM-1 samples 1 (a) and 2 (b) at 77 K. Adsorption points are marked by filled symbols and desorption points by empty symbols. B: Pore size distributions employing NLDFT model of samples 1 (c) and 2 (d).

The ^{13}C CP MAS NMR spectrum for LHMM-1 sample 2 is shown in Figure 6. The material exhibits strong signals at 10.3, 20.1, 23.2, 43.2, 54.9, 75.9, 115.1, 121.4, 145.2, 168.6 and 174.9 ppm due to the different carbon atoms of LHMM-1 framework. ^{13}C NMR of LHMS materials synthesized in the presence of CTAB as template with identical silica precursor **I**[12] also exhibited similar signals due to different C atoms. Thus this result indicates that the diimine fluorophore (**I**) is covalently linked to the silica inside the supermicroporous framework structure. ^{29}Si MAS NMR spectra of the organic-inorganic hybrid materials are often been used for assigning the chemical environment around the Si atoms.[1a] Typical ^{29}Si MAS NMR spectra of LHMM-1 sample 2 is shown in Figure 7. Downfield chemical shifts at –49.9, –57.8 and –67.9 ppm along with signals

at –81.2 ppm are observed. For the diimine fluorophore containing hybrid mesoporous silica LHMS-1 ^{29}Si peaks also exhibited similar chemical shifts of ca. –66.8 ppm and –57.9 ppm corresponding to the T^3 [$(OSi)_2$**Si**-R–**Si**$(OSi)_3$] and T^2 [$(OH)_2(OSi)$**Si**-R–Si$(OSi)_2(OH)$] species.[12] Additional peaks at δ = –49.9 ppm and –81.2 ppm could be attributed to the T^1 [$(OH)_3(OSi)$**Si**-R–Si$(OSi)_2(OH)$] and Q^1 silica species [**Si**$(OSi)(OH)_3$] type species in LHMM-1. Origin of Q^1 peak suggested that for a part of **I** species (12.7 wt.-%) Si–C bond cleavage occurred during high temperature (343 K) solvothermal synthesis. Thus this result clearly indicated the incorporation of diimine bridges inside the novel organic-inorganic hybrid framework of LHMM-1.

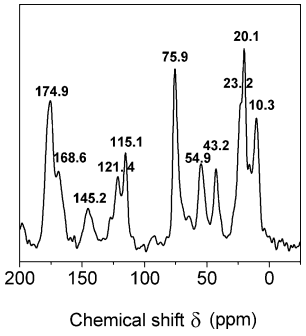

Figure 6. ^{13}C solid state CP MAS NMR spectra of LHMM-1 acid-treated sample 2.

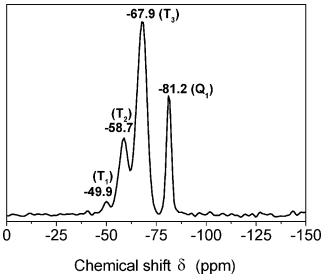

Figure 7. ^{29}Si solid state MAS NMR spectra of LHMM-1 acid-treated sample 2.

UV-visible spectroscopy can be used for characterizing the optical absorbance of the diimine moiety present in the LHMM-1 framework in the presence of proton or metal cations. Figure 8 shows the UV-visible diffuse reflectance spectra of acid-exchanged, base-exchanged and Fe^{3+}, Zn^{2+}, Cd^{2+} and Hg^{2+}-exchanged derivatives of sample 2 as well as that of diimine precursor **I**. All these samples exhibited three major UV/Vis absorption bands in the range 200–600 nm. Diimine precursor **I** shows very strong absorption bands at 241 and 348 nm and a weak one at 446 nm.[12] For all metal ion exchanged samples, mild shifts of the absorption bands are observed. This could be attributed due to the ligand chelation, which leads to ligand-to-metal charge transfer (LMCT) bands in addition to the $\pi \rightarrow \pi^*$ transitions of the chromophoric phenolic diimine.[16] Three strong absorption bands appeared at 252, 352 and 445 nm for the base-exchanged sample. For the acid, Fe^{3+} and Zn^{2+}exchanged samples the band at 348 nm is suppressed, whereas for the ammonia-treated, Cd^{2+} and Hg^{2+}-exchanged samples this peak intensity has been considerably enhanced. In the presence of acid the imine-N get protonated and thus their respective exited state energy also changes. This spectroscopic result further supports the assumption that the bridging diimine fluorophore moiety is present inside the LHMM-1 framework.

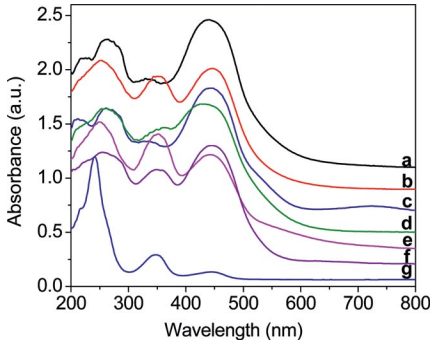

Figure 8. UV/Vis diffuse reflectance spectra of LHMM-1 sample 2: acid-exchanged (a), NH_3-treated (b), Fe^{III} exchanged (c), Zn^{II} exchanged (d), Cd^{II} exchanged (e), Hg^{II} exchanged (f) and pure Schiff base **I** (g).

Luminescence Property

The emission properties of the supermicroporous LHMM-1 samples were studied in solid state at room temperature. Figure 9 shows the photoluminescence (PL) spectra of the diimine precursor **I** and LHMM-1 samples (acid- and base-exchanged) and their Fe^{3+}, Zn^{2+}, Cd^{2+} and Hg^{2+}-exchanged derivatives. These samples showed single broad and strong emission band between 450 to 650 nm upon excitation at 350 nm light source. The emission spectra of all the metal-exchanged samples are distinctly red-shifted to higher wavelength with considerable change in intensity. Interestingly from the base-exchanged sample all other samples showed distinct red shifts in emission maxima. On protonation a pronounced red shift of ca. 38 nm together with a large enhancement in emission intensity was observed. Fe^{III}-exchanged sample showed maximum red shift of ca. 49 nm. For Zn^{II}, Cd^{II} and Hg^{II}-exchanged samples these shifts were ca. 21, 15 and 33 nm, respectively. Stronger chelation of Fe^{III} with phenolic OH and imine-N atoms could be attributed to the stabilization of the excited energy state for the Fe^{III} exchanged sample, resulting in a large red shift of the emission band.

The time-correlated single-photon counting (TCSPC) experiments were performed on different ion-exchanged LHMM-1 samples. LHMM-1 samples were excited with 350 nm light and their respective PL decays were monitored at the peak of the emission. The emission decays for these acid- and base-exchanged LHMM-1 samples are shown in Figure 10. The observed emission decay profiles can be simulated by using the multiexponential model.[17,18] The resulting decay times, τ_i, the average decay lifetimes, τ_{ave} and the values of the goodness-of-fit parameter χ^2_R,[18] are listed

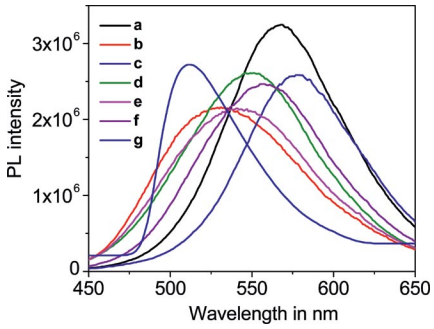

Figure 9. Photoluminescence spectra of LHMM-1 sample 2: acid-exchanged (a), NH_3-treated (b), Fe^{III} exchanged (c), Zn^{II} exchanged (d), Cd^{II} exchanged (e), Hg^{II} exchanged (f) and pure Schiff base **I** (g), excited at 350 nm.

in Table 3 for the decays corresponding to different ion exchanged LHMM-1 samples. This result suggested that acid exchanged and Fe^{III}-exchanged LHMM-1 samples has much larger emission lifetime than the base exchanged or Zn^{II} or Cd^{II}-exchanged samples.

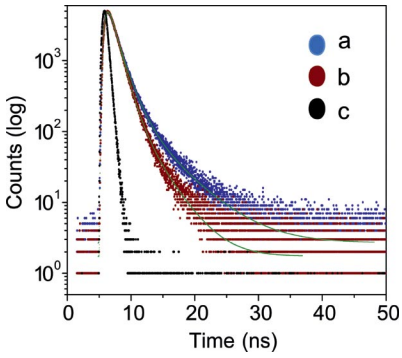

Figure 10. Representative time-resolved fluorescence decay profiles of LHMM-1 sample 2 (λ_{ex} = 350 nm): acid-exchanged (a), NH_3-treated (b). The sharp profile is the lamp profile (c).

Table 3. Emission maximum, component of emission lifetime (τ_i) and the preexponential factor (a_i)[a] for the decays corresponding to different ion exchanged LHMM-1 samples.

Sample type	Emission maximum [nm]	τ_1 [ns]	τ_2 [ns]	τ_3 [ns]	χ^2	τ_{ave} [ns]
Acid-exchanged	568	0.79 (30.99)	1.61 (56.89)	4.98 (12.11)	1.103	2.648
Base-exchanged	530	1.14 (87.17)	3.17 (12.83)	–	1.135	1.729
Fe^{III}-exchanged	578	0.65 (22.97)	1.38 (63.95)	4.42 (13.08)	1.023	2.95
Zn^{II}-exchanged	549	1.09 (80.11)	3.72 (19.89)	–	1.166	2.296
Cd^{II}-exchanged	541	0.408 (6.93)	1.25 (85.50)	3.97 (7.57)	1.055	1.817
Hg^{II}-exchanged	557	1.17 (78.78)	3.89 (21.22)	–	1.228	2.45

[a] Preexponential factors for each component are given in parentheses.

Ion-Exchange Property

In Table 4 we have summarized our ion-exchange results for our fluorophore grafted LHMM-1 material. Ion exchange efficiency and distribution coefficient (K_d) for Fe^{3+}, Zn^{2+}, Cd^{2+} and Hg^{2+} are calculated form their respective concentrations before and after ion exchange measurements. For each of these metal cations two sets of stock solutions of ca. 200 and 20 ppm are taken before the ion-exchange analysis. For all these biologically relevant, environmentally demanding and heavy metal cations LHMM-1 showed very high cation removal efficiency (89–98 wt.-%). Formation of a chelate-type complex due to the coordination of metal cations with phenolic OH and imine-N donors could be responsible for the high K_d values for all these metal cations.[19,20] Figure 11 shows emission images from acid (a) and base-exchanged (b) LHMM-1 samples after UV light irradiation. It can be seen from these images that the fluorescence colors vary drastically from pale yellow to green during deprotonation. Thus the optical properties of the LHMM-1 samples are highly pH-dependent and reflect the effects of different metal cations (Fe^{3+}, Zn^{2+}, Cd^{2+} and Hg^{2+}). This can be observed with the naked eye. Thus our experimental results suggests that the diimine fluorophore **I** has been grafted inside the supermicroporous triclinic framework of LHMM-1. When this material is treated with metal salt solution, the phenolic diimine moiety can coordinate with metal cations and from chelating complex with phenolic OH and imine-N donors.[12] Formation of these chelating complexes thus responsible for the sensing and ion-exchange properties of these materials.

Table 4. Cation exchange efficiencies of LHMM-1 from different metal salt solutions.

Sample name	Solution (100 mL)	Cation content (ppm) before	Cation content (ppm) after	Cation removal % efficiency	Distribution coefficient (K_d)[a]
LHMM-1	Fe^{3+}	232.74	20.35	91.25	2.08×10^4
		24.23	0.47	98.06	1.01×10^5
	Zn^{2+}	208.66	18.41	91.17	2.06×10^4
		20.37	0.52	97.44	7.63×10^4
	Cd^{2+}	203.98	22.38	89.02	1.62×10^4
		20.16	0.59	97.07	6.63×10^4
	Hg^{2+}	208.93	23.04	88.97	1.61×10^4
		20.81	0.69	96.68	5.83×10^4

[a] Distribution coefficient (K_d) between solid and water phase: [cation adsorbed]/[cation in solution].

It is pertinent to mention that in our previous work on luminescent PMO material LHMS[12] we have synthesized mesoporous organosilica through a surfactant templating method using a mixture of this organosilane precursor and TEOS having a highly periodic mesoporous structure. However, the present work deals with the synthesis of crystalline supermicroporous organosilica by a non-templating method using the same organosilane precursor **I** alone. Although the same organosilane precursor has been used in both works, materials prepared (mesoporous with amorphous pore wall vis-à-vis supermicroporous with crystalline framework) and methods adopted (surfactant templating

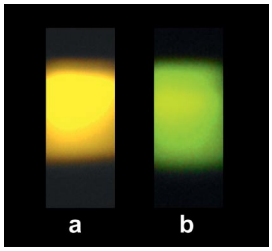

Figure 11. Representative photographic images of LHMM-1 sample 1, casted on quartz substrate: acid (a) and ammonia-treated (b), after UV light irradiation.

versus non-templating) are different in both cases. Their pore dimensions, crystal structure and surface properties differ considerably. The ion exchange properties of LHMM-1 also improved considerably from LHMS. As can be seen from Table 4, LHMM-1 has a much higher ion exchange efficiency (98.06 and 97.44% versus 80.4 and 72.5% for Fe^{3+} and Zn^{2+}, respectively) and K_d compared to the mesoporous LHMS materials. This could be attributed to the presence of a higher concentration of diimine fluorophore in LHMM-1 (100% versus 25% in LHMS sample 1) and also crystalline feature of the framework, which has been solved through wide-angle powder diffraction XRD data analysis here. Further, ^{13}C CP MAS, ^{29}Si MAS NMR, UV/Vis absorption and PL spectroscopic data for LHMM-1 and LHMS samples 1[12] showed considerable shifts of their peak positions and intensities although both materials have the same chemical composition. This could be originated from the pore size (supermicropore/mesopore) and crystallinity (triclinic/amorphous pore wall) in their respective nanostructures.

Conclusions

Based on the above results we can conclude that a novel microporous organic-inorganic hybrid organosilica material LHMM-1 has been synthesized solvothermally at 343 K without using any structure-directing agent. New framework structure of the LHMM-1 material is characterized by powder XRD, TEM and N_2 sorption analyses, which indicated the triclinic crystal structure and the presence of supermicropores with pore dimension of ca. 1.39–1.53 nm in this new triclinic structure. ^{13}C CP NMR, UV/Vis and PL spectroscopic analyses demonstrated the incorporation of organic fluorophore in this material. This fluorophore-grafted organic-inorganic hybrid material shows strong affinity toward metal cations like Fe^{3+}, Zn^{2+}, Cd^{2+} and Hg^{2+}, and thus can be very efficiently utilized as metal ion sensor. All these metal ion-exchanged LHMM-1 samples exhibit strong photoluminescence at room temperature and dependence of emission colors when exchanged with a particular metal cation.

Experimental Section

Materials: Bridged fluorescent organosilane precursor (Figure 1), **I** $(EtO)_3Si(CH_2)_3N{=}CH\text{-}C_6H_2(CH_3)(OH)\text{-}CH{=}N(CH_2)_3Si(OEt)_3$, has been synthesized through Schiff-base condensation between 2,6-diformyl-4-methylphenol (DFP) and (3-aminopropyl)triethoxysilane (APTES, Sigma Aldrich). Detail synthesis method has been given elsewhere.[12] All other chemicals, unless mentioned otherwise used in this investigation were of analytical grade and purchased from E. Merck. All the solutions for the salts $Zn(NO_3)_2$, $Fe(NO_3)_3$, $Cd(NO_3)_2$ and $HgCl_2$ of different metal ion were prepared in Millipore water.

Instrumentation: ^1H and ^{13}C NMR (liquid state) experiments were carried out on a Bruker DPX-300 NMR spectrometer. FT IR spectra of these samples were recorded between the ranges 400–4000 cm^{-1} using a Nicolet MAGNA-FT IR 750 Spectrometer Series II. Mass spectrometric data were acquired by the electron spray ionization (ESI) technique at 25–70 eV in a Micromass Q-tof-Micro quadruple mass spectrophotometer. Carbon, hydrogen and nitrogen contents were analyzed using a Perkin–Elmer 2400 Series II CHN analyzer. X-ray diffraction patterns of the powder samples were obtained with a Bruker AXS D8 SWAX diffractometer using Cu-K_α (λ = 0.15406 nm) radiation, in the 2-theta value range of 2–35. Nitrogen adsorption/desorption isotherms were obtained by using a Bel Japan Inc. Belsorp-HP at 77 K. Prior to gas adsorption, samples were degassed for 6 h at 393 K under high vacuum conditions. A JEOL JEM 6700F field emission scanning electron microscope with an EDS attachment was used for the determination of morphology and chemical composition. Solid-state ^{29}Si MAS NMR measurement was performed on a Varian VNMR6.1C (300 MHz) spectrometer at a spinning rate of 5 kHz and a resonance frequency of 59.59 MHz with a 90^0 pulse length of 3.6 μs and a recycle time of 5 s. The chemical shifts for ^{29}Si spectra were referenced to TMS at 0 ppm. Solid state ^{13}C CP/MAS NMR measurement was performed at a spinning rate of 4 kHz and a resonance frequency of 75.43 MHz with a recycle time of 5 s. Thermogravimetry (TG) and differential thermal analyses (DTA) of the samples were carried out between the temperature ranges 298 K to 1073 K in a TA Instruments thermal analyzer TA-SDT Q-600. Elemental analyses of the solid and exchanged solutions were estimated by using a Shimadzu AA-6300 atomic absorption spectrophotometer (AAS) fitted with a double-beam monochromator. UV/Vis diffuse reflectance spectra were recorded between the ranges 200–800 nm on a Shimadzu UV 2401PC with an integrating sphere attachment. $BaSO_4$ was used as background standard. The emission spectra were recorded between the ranges 450–650 nm on a Fluoromax-P Horiba Jobin–Yvon luminescence spectrometer, using a solid sample holder at room temperature. The powder samples were pressed to form smooth, opaque flat disks for the optical study. Fluorescence lifetimes were determined by the time-resolved intensity decay method of time-correlated single-photon counting (TCSPC) by using a Fluoro Cube HORIBA JOBIN YVON instrument with an excitation wavelength of 350 nm from a diode laser.

Synthesis of Luminescent Hybrid Microporous Material (LHMM-1): LHMM-1 has been synthesized by controlled acid hydrolysis of bridging fluorescent organosilane precursor **I**, followed by the further treatment of this acid hydrolyzed product with ammonia vapor. In a typical synthesis a solution of **I** (2.85 g, 0.005 mol) in dry methanol (25 mL) was placed under nitrogen atmosphere in a two-necked round-bottom flask equipped with a condenser and an addition funnel. Then 0.8 g (0.008 mol) of 62% HNO_3 solution was added to it dropwise whilst stirring, which was followed by addition of 1.5 g (0.083 mol) of water. The reaction mixture was kept at reflux (343 K) for 2 h and allowed to cool to room temperature. The dark orange solution was then poured into a petri-dish to evaporate the solvent. On evaporation of the solvent from this reaction mixture crystal like solid LHMM-1 formed. This sample was

designated as LHMM-1 sample 1. This as-synthesized orange solid was kept 6 h in a closed container containing 20 mL of 25% aqueous NH_4OH solution in such a way that the solid product did not come to direct contact with the NH_4OH solution. After 6 h the resultant orange solid was crushed to give a powder, washed for several times with water, then dried under a vacuum. This NH_3 vapor-treated sample was designated as LHMM-1 sample 2. The protonated form was prepared by treating 0.1 g of sample 2 with 20 mL, 0.1 N aqueous HCl. Treatment of this acid-treated sample (0.1 g) with 20 mL, 0.1 M aqueous NH_3 solution in water resulted in the base-exchanged sample 2.[12] The metal-exchanged samples were prepared by treating the base-exchanged samples (0.1 g) with 20 mL, 0.1 M aqueous solutions of metal salts.

Ion-Exchange Measurements: For the ion-exchange measurements, 0.05 g of base-exchanged sample 2 was added to 100 mL aqueous ion solution (Zn^{2+}, Fe^{3+}, Cd^{2+} or Hg^{2+}); this solution was stirred for 2 h at room temperature, then filtrated. The concentrations of the cations in the initial solution and final filtrate were determined by AAS. By subtracting the concentration of an ion in the filtrate from the initial solution, exchanged ion concentration and thus anion removal efficiency was determined.

Acknowledgments

A. B. wishes to thank the Department of Science and Technology (DST), New Delhi for extramural research grants. A. D. thanks the Council of Scientific and Industrial Research (CSIR), New Delhi for a junior research fellowship.

[1] a) S. Inagaki, S. Guan, Y. Fukushima, T. Ohsuna, O. Terasaki, *J. Am. Chem. Soc.* **1999**, *121*, 9611–9614; b) T. Asefa, M. J. MacLachlan, N. Coombs, G. A. Ozin, *Nature* **1999**, *402*, 867–871; c) R. M. Grudzien, B. E. Grabicka, S. Pikus, M. Jaroniec, *Chem. Mater.* **2006**, *18*, 1722–1725.

[2] a) A. Stein, B. J. Melde, B. T. Holland, C. F. Blanford, *Chem. Mater.* **1999**, *11*, 3302–3308; b) A. Stein, B. J. Melde, R. C. Schroden, *Adv. Mater.* **2000**, *12*, 1403–1419; c) A. Sayari, S. Hamoudi, *Chem. Mater.* **2001**, *13*, 3151–3168; d) R. Anwander, *Chem. Mater.* **2001**, *13*, 4419–4438; e) K. Yamamoto, T. Sakata, Y. Nohara, Y. Takahashi, T. Tatsumi, *Science* **2003**, *300*, 470–472.

[3] a) S. Inagaki, S. Guan, T. Ohsuna, O. Terasaki, *Nature* **2002**, *416*, 304–307; b) E.-B. Cho, D. Kim, M. Jaroniec, *Chem. Mater.* **2008**, *20*, 2468–2475; c) E.-B. Cho, D. Kim, *J. Phys. Chem. Solids* **2008**, *69*, 1142–1146.

[4] a) H.-B. Fa, L. Zhao, X.-Q. Wang, J.-H. Yu, Y.-B. Huang, M. Yang, D.-J. Wang, *Eur. J. Inorg. Chem.* **2006**, *21*, 4355–4361; b) L. Zhang, J. Liu, J. Yang, Q. Yang, C. Li, *Chem. Asian J.* **2008**, *3*, 1842–1849.

[5] a) R. Casas, E. Aznar, M. D. Marcos, R. Martinez-Manez, F. Sancen, J. Soto, P. Amor, *Angew. Chem. Int. Ed.* **2006**, *45*, 6661–6664; b) J. L. Soo, R. B. Doo, S. H. Won, S. L. Shim, H. J. Jong, *Eur. J. Inorg. Chem.* **2008**, 1559–1564; c) K. Sarkar, K. Dhara, M. Nandi, P. Roy, A. Bhaumik, P. Banerjee, *Adv. Funct. Mater.* **2009**, *19*, 223–234.

[6] a) K. Nakajima, I. Tomita, M. Hara, S. Hayashi, K. Domen, J. N. Kondo, *Adv. Mater.* **2005**, *17*, 1839–1842; b) M. Benitez, G. Bringmann, M. Dreyer, H. Garcia, H. Ihmels, M. Waidelich, K. Wissel, *J. Org. Chem.* **2005**, *70*, 2315–2321; c) J. Chakraborty, M. Nandi, H. Mayer-Figge, W. S. Sheldrick, L. Sorace, A. Bhaumik, P. Banerjee, *Eur. J. Inorg. Chem.* **2007**, 5033–5044; d) C. González-Arellano, A. Corma, M. Iglesias, F. Sánchez, *Eur. J. Inorg. Chem.* **2008**, 1107–1115.

[7] a) R. Szostak, *Molecular Sieves: Principles of Synthesis and Identification*, Van Nostrand Reinhold, New York, **1989**; b) A. Corma, *Chem. Rev.* **1997**, *97*, 2373–2419.

[8] C. T. Kresge, M. E. Leonowicz, W. J. Roth, J. C. Vartuli, J. S. Beck, *Nature* **1992**, *359*, 710–712.

[9] a) X. S. Zhao, G. Q. Lu, G. J. Millar, *Ind. Eng. Chem. Res.* **1996**, *35*, 2075–2090; b) D. Zhao, J. Feng, Q. Huo, N. Melosh, G. H. Fredrickson, B. F. Chmelka, G. D. Stucky, *Science* **1998**, *279*, 548–552; c) Y. Wan, D. Zhao, *Chem. Rev.* **2007**, *107*, 2821–2860.

[10] a) L. Tosheva, V. P. Valtchev, *Chem. Mater.* **2005**, *17*, 2494–2513; b) C. Bouvy, F. Piret, W. Marine, B. L. Su, *Chem. Phys. Lett.* **2007**, *433*, 350–354; c) D. Chandra, S. Mridha, D. Basak, A. Bhaumik, *Chem. Commun.* **2009**, 2384–2386.

[11] K. Ogawa, S. Chemburu, G. P. Lopez, D. G. Whitten, K. S. Schanze, *Langmuir* **2007**, *23*, 4541–4548.

[12] D. Chandra, T. Yokoi, T. Tatsumi, A. Bhaumik, *Chem. Mater.* **2007**, *19*, 5347–5354.

[13] a) N. Mizoshita, Y. Goto, T. Tani, S. Inagaki, *Adv. Funct. Mater.* **2008**, *18*, 3699–3705; b) S. M. Bruno, A. C. Coelho, R. A. S. Ferreira, L. D. Carlos, M. Pillinger, A. A. Valente, P. Ribeiro-Claro, I. S. Gonçalves, *Eur. J. Inorg. Chem.* **2008**, 3786–3795.

[14] a) B. G. Shpeizer, V. I. Bakhmutov, A. Clearfield, *Microporous Mesoporous Mater.* **2006**, *90*, 81–86; b) D. Chandra, A. Bhaumik, *Microporous Mesoporous Mater.* **2008**, *112*, 533–541.

[15] *Atlas of Zeolite Framework Types*, 5th revised edition, **2001**, Ch. Baerlocher, W. M. Meier, D. H. Olson (Eds.).

[16] a) H.-F. Xiang, S.-C. Chan, K. K.-Y. Wu, C.-M. Che, P. T. Lai, *Chem. Commun.* **2005**, 1408–1410; b) F. Pelascini, F. Peruch, P. J. Lutz, M. Wesolek, J. Kress, *Eur. Polym. J.* **2005**, *41*, 1288–1295.

[17] J. R. Lakowich, *Principles of Fluorescence Spectroscopy*, 2nd ed., Kluwer Academic/Plenum Publishers, New York, Boston, Dordrecht, London, Moscow, **1999**.

[18] M. Jones, J. Nedeljkovic, R. J. Ellingson, A. J. Nozik, G. Rumbles, *J. Phys. Chem. B* **2003**, *107*, 11346–11352.

[19] H. Yoshitake, T. Yokoi, T. Tatsumi, *Chem. Mater.* **2002**, *14*, 4603–4610.

[20] D. Chandra, A. Bhaumik, *J. Mater. Chem.* **2009**, *19*, 1901–1907.

Received: June 25, 2009
Published Online: August 14, 2009

